Composites Science and Technology 239 (2023) 110046

Contents lists available at ScienceDirect

Composites Science and Technology

journal homepage: www.elsevier.com/locate/compscitech

Dissolution dynamics of woven all-silk composites fabricated in the ionic liquid 1-ethyl-3-methylimidazolium acetate

Xin Zhang, Michael E. Ries *, Peter J. Hine

School of Physics and Astronomy, University of Leeds, Woodhouse Lane, Leeds, LS2 9JT, UK

ARTICLE INFO

Keywords:
Natural fibre composites
Bio composites
Woven silk composites
Dissolution activation energy
Mechanical properties

ABSTRACT

Single layer woven all-silk composites (ASCs) have been prepared using the ionic liquid 1-ethyl-3-methylimidazolium acetate ([C2mim][OAc]), with the dissolution carried out under various times and temperatures. Cross sectional images revealed the dissolved and coagulated silk matrix were formed along both fibre directions with thicker matrix layer observed along warp direction. Radial integration utilising the second Legendre polynomial function (P_2) were conducted on the collected intensity distribution curves attained from WAXD azimuthal scans, enabling the quantitative measurement of the average orientation of crystals. A simple linear mixing rule was employed to correlate the coagulated matrix (V_m) with respective P_2 values, leading to the calculation of V_m. Time–temperature superposition (TTS) was verified through the construction of master curves, from which the dissolution was found to have Arrhenius-like behaviour allowing the determination of dissolution activation energy (E_a). The three measured tensile properties were all found to follow TTS principle, thus yielding another two methods to determine E_a. Five different methods point to an average E_a value of 93 ± 2 kJ/mol. Additionally, the dissolution rates and activation energies of single and woven silk were compared. The master curves constructed in this study may provide a guidance for future design of silk fibre reinforced composites with desired properties.

1. Introduction

Increasing demand for lightweight, biodegradable and biocompatible materials have moved industries to focus on natural fibre composites in the past few years [1,2]. In polymer composites area, natural fibres (both plant and animal based) are increasingly being used in many industries [3,4]. The main interests come from its low density and cost, high specific strength, sustainability, and renewability. In recent years, natural fibre composites are becoming attractive alternatives to glass and carbon fibre reinforced polymer composites [5]. Among animal fibres, silk fibres have attracted a large amount of interests particular due to a combination of biodegradability, biocompatibility and remarkable mechanical properties [6,7]. Bombyx mori (B.mori) silkworm contains silk fibroin (SF) approximately 5–10 μm in diameter [8]. The SF nanofibrils are composed of proteinaceous components, a heavy chain (H-chain) fibroin (of ca. 350 kDa) linked to a light chain (L-chain) fibroin (of ca. 26 kDa) via disulphide bonds at the C-terminus. The structural units of H-chain are blocks of (G-A-G-A-G-S)n (G = glycine, A = alanine, S = serine) that are packed into highly-stable hydrophobic β-sheet nanocrystals, whereas the L-chain is hydrophilic and elastic [9].

The dissolution of silk requires disruption of the hydrogen bonds and van der Waals interactions present. Due to the presence of a large number of hydrogen bonds, and 75% of amino acids within SF being nonpolar and hydrophobic, this leads to SF being insoluble in water or in most organic solvents [10]. Ionic liquids (ILs) are a class of solvents that are composed of cations and anions, and recognised as molten salts with negligible vapour pressure [11]. In combination with their other properties, high thermal stability, high tunable properties and potential recyclability, ionic liquids have become the potential 'green' solvents for use in industry [12,13]. ILs have been proposed and applied as promising solvents for dissolving biomacromolecules such as cellulose, chitin and keratin [14–16]. In 2004, Phillips et al. studied the dissolution of SF using an ionic liquid for the first time [17]. The results showed that the more destructive the IL is to the hydrogen bonds in crystalline domains of silk fibres, the higher the solubility. Additionally, the secondary structure of SF in ionic liquids can be tuned by ethanol, methanol or other organic solvents during the coagulation process, enabling the preparation of materials with a range of applications such as tissue engineering, drug delivery system, and silk-reinforced composites [7,18,19].

* Corresponding author.
E-mail addresses: cm16xz@leeds.ac.uk (X. Zhang), m.e.ries@leeds.ac.uk (M.E. Ries), p.j.hine@leeds.ac.uk (P.J. Hine).

https://doi.org/10.1016/j.compscitech.2023.110046
Received 7 October 2022; Received in revised form 6 April 2023; Accepted 14 April 2023
Available online 24 April 2023

Silk fibres used as reinforcement in combination with a polymer matrix have been widely discussed in many studies. Shubhra, Q.T.H et al. have fabricated silk fibre reinforced polypropylene matrix composites; limited strength values were obtained likely due to lack of fibre–matrix adhesion [20]. Silk fibres reinforced with different polymer matrices Co-PP (copolypropylene), PP-g-MA (polypropylene grafted with maleic anhydride), PBS (polybutylene succinate), PBSa (polybutyl succinate/adipate) were compared; high toughness composites can be obtained by reinforcing ductile silk fibres with thermoplastic matrices which have high failure strain [21]. However, only a very few studies have so far been conducted on the mono-composite area, where silk fibre is both the reinforcement and the matrix phase. Studies have pointed out mono-composites present a few advantages comparing to fibres reinforced with polymer matrices composites, such as (i) the enhanced interfacial adhesion between fibre and matrix phase due to the pure chemical functionality; (ii) the homogeneity in constituents can potentially lead to easier recycling process [22,23]. Generally, there are mainly two strategies for preparing all silk composites (ASCs): (a) one-step method, partially dissolve silk fibres and regenerating the dissolved fibres to form the matrix; (b) two-step method, completely dissolve silk fibres to form a solution followed with regenerating the solution to form matrix, embedded with additional silk fibres as reinforcement. Yuan Q.Q et al. have used the two-step method to prepare all silk composites, embedding silk fibres in a fibroin matrix by solution casting; good strength properties were obtained [24].

Additionally, studies on the kinetics and mechanisms of the dissolution of silk are still very limited. Laity and Holland [25] have reported that the rheology of the liquid feedstock of B.mori changes with temperature, and was found to have activation energy (E_a) of flow range from 30.9 to 55.4 kJ/mol. Some researchers have done thermal analyses on silk, Liu.Y et al. [26] reported the decomposition E_a for the native silkworm silk, ranging 194–217 kJ/mol; Liu.Q et al. [27] studied the decomposition E_a for silk fibroin films and found values between 158 to 190 kJ/mol. However, to the best of author's knowledge, there are no studies that investigate the dissolution dynamics of woven silk fabrics when using the partial dissolution method to prepare woven all silk composites.

In this study, partial dissolution method was applied to fabricate woven all silk composites, with an imidazolium-based ionic liquid ([C2mim][OAc]) selected as the solvent. The partial dissolution of woven silk fabric was carried out at a range of times and temperatures, with the remaining silk fibres serving as the reinforcement phase, while the dissolved and coagulated silk served as the matrix phase. The resultant woven ASCs were characterised using different techniques. By analysing azimuthal WAXD scan results, we discovered that the dissolution can be tracked through following the orientation changes of nanocrystallites within each obtained woven ASC. A time–temperature shifting method was applied to the determined P_2 values. Here, to author's knowledge, we have for the first time discovered that the dissolution of woven silk fabrics displays Arrhenius-type behaviour, and thus allowing the corresponding dissolution activation energy (E_a) to be calculated. Meanwhile, the volume fraction of dissolved and coagulated matrix (V_m) can be calculated through the employment of a linear mixing rule. In addition, tensile behaviour of the resultant woven ASCs were measured, with the time–temperature equivalence on the measured parameters verified through the construction of master curves using the same shifting method. To the best of our knowledge, this is the first report that demonstrates the tensile properties of woven all-silk composites can be tailored through the control of dissolution times and temperatures. The dissolution activation energies were subsequently calculated from the respective Arrhenius plots. The applicability of the rule of mixtures was examined. In combination with our previous study on single silk fibre dissolution, the V_m master curves of single silk fibres and woven silk fabrics were compared in one graph, and the dissolution activation energies and the dissolution rates were compared. Master curves of measured parameters constructed in this study can provide a clear guidance for designing silk-based composites with desired properties.

2. Experiments and methodology

2.1. Materials

Degummed B. mori silk fibre yarn was purchased online (Mulberry Undyed Spun Silk from Airedale Yarns, UK) and stored in a cool dry place before use. Silk fibre yarn was then hand woven into a silk fabric by following a plain weave process. The ionic liquid 1-ethyl-3-methylimidazolium acetate [C2mim][OAc] was purchased from Sigma–Aldrich, with a purification of 97% and a water content of 0.53%. Methanol was chosen to use as the coagulation bath since it can exhibit a strong crystallisation capability and provide strong coagulation strength [28].

2.2. Fabrication of woven all silk composites (ASCs)

Woven silk fabrics were cut into multiple 50 mm × 20 mm strips, ready for preparing single layer woven ASCs. Next, a poly(tetrafluoroethylene) (Teflon) dish was filled with excess [C2mim] [OAc], followed by being put into vacuum oven for 1 h to allow the IL to be preheated to a chosen temperature. Then the cut woven strips were fully immersed in the preheated IL bath (yielding a 0.7 % w/v), inside the vacuum oven for the designed length of time. According to the results from our previous studies on the dissolution of single silk fibres [29], temperatures at 40, 50 or 60 °C were the suggested correct range for conducting the dissolution of woven silk fabrics.

After the dissolution finished, the woven silk strips were immediately transferred into the methanol bath, to allow the dissolved silk filaments to coagulate, and form a silk matrix that surrounds the remaining undissolved silk. The used [C2mim][OAc] was collected to be recycled. Next, the woven ASCs were soaked in the methanol bath for 2 days with changing the medium twice, to remove any contained IL. Finally, the woven ASCs were dried in hot press for 1 h at 100 °C with contact pressure approximately at 0.15 MPa.

2.3. Structure and morphology characterisations

The morphologies of the unprocessed woven silk fabric and the woven ASCs were characterised using an optical microscope (BH2-UMA, Olympus Corporation, Japan). The surface morphology was examined in transmission mode, while the cross-sectional images were captured in reflection mode. Woven silk fabrics were embedded in an epoxy resin (EpoxiCure2, BUEHLER), followed by hardening for 3 h at 50 °C in an oven. Then, the surface of the resin was ground and polished to reveal the woven ASCs cross sections.

2.4. Wide-angle X-ray diffraction characterisation

X-ray studies of the orientation of the distribution of nanocrystallites of the woven ASCs and the coagulated SF film were performed at ambient temperature, using an X-ray diffractionmeter (DRONEK 4-AXES, Huber Diffracionstechnik GmbH & Co. KG, Germany) equipped with Cu Kα radiation generated at 40 kV and 30 mA (λ = 1.54 Å). The system was operated in transmission mode. The azimuthal scan was carried out by fixing on a specific Bragg peak where the maximum crystalline intensity from the 2θ scan was found for unprocessed woven silk fabric (20.6°, from the strong and clearly identified (020) diffraction plane) [30]. The intensity distribution was then collected by varying the azimuthal angle from - 90° to 90° (0° = vertical), with a scanning rate of 2°/min. It is expected that an amorphous (randomly oriented) phase would give a constant intensity at all angles while the crystalline regions (representative of the silk fibres) would show a peak due to their preferred orientation.

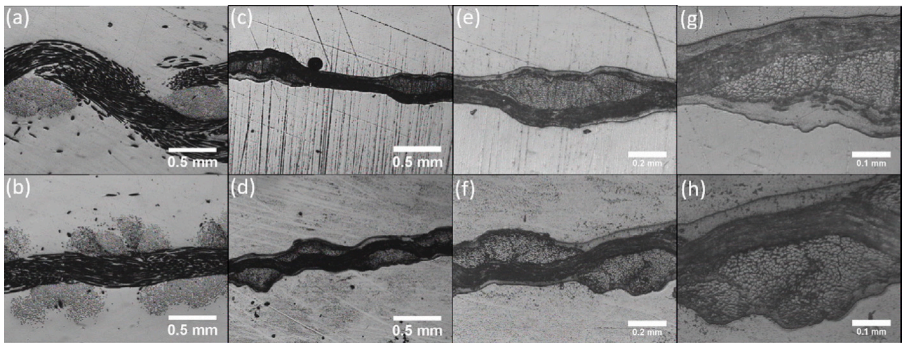

Fig. 1. Optical microscope cross-sectional images of unprocessed (a and b) and partially dissolved at 40 °C–5 h (c–h) woven silk fabrics, when warp bundles (a,c,e,g) and weft bundles (b,d,f,h), perpendicular to the plane.

2.5. Tensile properties tests

Tensile properties of the woven ASCs were measured using an Instron 5565 universal test machine equipped with a 10 kN calibrated load cell at room temperature. The gauge length and the speed of the instrument were set to 20 mm and 2 mm/min, respectively. At least 3 strips at the size of 50 mm × 5 mm were measured from each woven ASC sample, and an average value was calculated along with a standard uncertainty. The tensile strength and elongation at break values were measured from the stress–strain curves, with Young's modulus calculated from the corresponding initial linear strain range (0.0050–0.0100). A three-point bending flexural test was performed to test the flexural modulus of the completely dissolved and coagulated SF film (as it was too brittle to be gripped for a tensile test). The same instrument was used with a cross-head speed at 2 mm/min and a bending span of 20 mm. The value of flexural modulus was again taken from the average of testing results from three specimens.

3. Results and discussion

3.1. Microstructure of woven ASCs

The plain woven silk fabric is composed of individual fibre threads in two directions, which are named 'warp' and 'weft' in weaving. The surface morphology of the unprocessed woven silk fabric is presented in Fig. S1a and b. The cross-sectional images of unprocessed and partially dissolved (40 °C–5 h) woven silk fabrics were taken using optical microscopy and shown in Fig. 1.

Compared to the unprocessed woven fabric (Fig. 1a and b), Fig. 1c and d reveal that the overall area of the remaining lenticular shape of the fibre core and the width of the bundle that is parallel to the plane, from woven ASC (40 °C–5 h) were decreased. It is expected that as the dissolution progresses, the dissolved fibres are turning into matrix, so the proportion of matrix phase is increased, which can be seen more clearly in higher magnification images (Fig. 1e-h). Especially in Fig. 1g and h, a layer of the matrix phase is formed, which appears as a lighter colour and surrounds the outer surface of the weft and warp direction fibre core. Interestingly, thicker layer of matrix can be seen along warp direction fibre core. Through using the software Image J, the thickness of the matrix layer was measured. Under the same dissolution condition, the ratio of the matrix thickness along the fibre core between warp and weft yarns was found close to ~2:1 (warp : weft). One of the reasons could be the distance between each warp bundles are significant larger than that of weft bundles, thus more space is left for matrix to be generated.

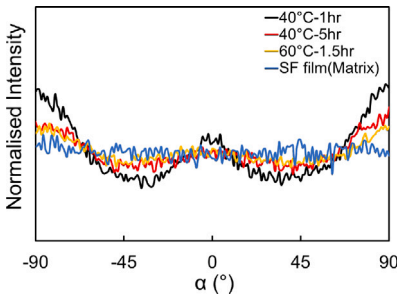

Fig. 2. Azimuthal diffraction curves for woven ASCs obtained from 40 °C–1 h, 40 °C–5 h, 60 °C–1.5 h and the coagulated SF film.

3.2. Characterisation of woven ASCs crystalline orientation

The woven ASCs were characterised by WAXD prior and subsequent to dissolution. It is expected that upon dissolution, the crystalline structure/orientation of the resultant woven ASCs, particularly for the coagulated SF film, will be different to the unprocessed woven silk fabric. Fig. 2 represents WAXD azimuthal scans of partially dissolved woven ASCs including processed at lowest temperature and shortest time −40 °C for 1 h, and 40 °C for 5 h, 60 °C for 1.5 h; as well as the coagulated SF film from [C2mim][OAc] solution with 5 wt% silk fibre. Significant change in the intensity distribution can be observed. The change in the intensity distribution correlates to the difference between the preferred aligned crystalline orientation of the woven ASC prepared at lowest temperature and shortest time and the randomly oriented crystals in the SF film (matrix phase). The diffraction curves were normalised to give the same total area.

As mentioned in Section 2.4, WAXD azimuthal profiles were collected by scanning through azimuthal angles from −90 to 90° from the reflection plane (020) (2θ = 20.6°). There were three peaks in the diffraction curve, located at α = −90°, 0° and 90°, corresponding to the weft, warp and weft direction respectively; with the warp direction vertical at α = 0°. It can be seen that the partially dissolved woven ASC at 40 °C for 1 h shows the highest peak intensity at α = −90°, 0° and 90°, whereas the coagulated SF film shows a flat distribution curve throughout the whole scanning angle, confirming random crystalline orientation. Compared to the woven ASC at 40 °C for 1 h, the normalised peak intensity at the α angle = −90° and 90°, of the other partially dissolved woven ASCs processed at longer time or higher temperature is lower, and tending to flatten between −45° and 45°, while its baseline (from the coagulated SF component) is higher. The changes directly corresponded to the percentage of crystalline component being dissolved by the IL and transformed into a randomly oriented structure through the coagulation process. The background diffraction intensity of azimuthal scan for the reflection plane (020) was measured and subtracted.

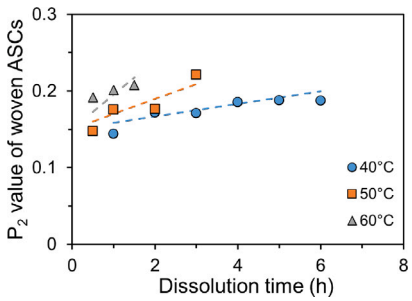

Fig. 3. Average P_2 values calculated from WAXD azimuthal scans for woven ASCs dissolved in [C2mim][OAc] at various times and temperatures; the dashed lines are guide for the eye.

The orientation factor (P_2), is an important parameter directly related to the physical properties of the woven silk fabric, since it quantifies the axial orientation distributions of nanocrystallites. Accordingly, radial integration of the experimentally measured intensity distributions on the Debye ring around the (020) equatorial reflection can be applied to determine the average orientation of the nanocrystallites within the woven ASCs using the 2nd Legendre polynomial function, as given in Eq. (1) [31].

$$P_2 = \frac{1}{2}(3\langle\cos^2\alpha\rangle - 1) \tag{1}$$

where $\langle\cos^2\alpha\rangle$ is the average cosine squared value of the azimuthal angle α, in a two dimensional azimuthal scan, and calculated using Eq. (2).

$$\langle\cos^2\alpha\rangle = \frac{\int_{-\pi/2}^{\pi/2} I(\alpha)\cos^2\alpha \mathrm{d}\alpha}{\int_{-\pi/2}^{\pi/2} I(\alpha)\mathrm{d}\alpha} \tag{2}$$

where I (α) is the scattered intensity at α along the diffraction profile. The measured I (α) value was taken from the obtained WAXD scatter curve, and directly put into a built Excel spreadsheet, to calculate $\langle\cos^2\alpha\rangle$ and P_2 by using Eqs. (1) and (2) shown above, respectively.

The orientation factors of the nanocrystallites for the woven ASC obtained from processing at various times and temperatures were determined from their distribution curves by using Eq. (1), and the results are given in Fig. 3. It is expected that, the dissolution continuously disrupts the preferentially oriented nanocrystallines, thus will influence the crystal orientation and subsequently P_2 values. Fig. 3 implies a P_2 value of 0.14 for the woven ASC obtained from early dissolution stage (40 °C for 1 h). Besides, theoretically, the P_2 value should be equal to 0.25 for a random 2D isotropic structure in woven fabrics. As the dissolution progress, the amount of randomly oriented component would increase, and eventually become fully isotropic. Consequently, a increased value of P_2 is expected, from 0.14 (woven ASC processed at lowest time and temperature) to 0.25 (random 2D isotropic). As expected, Fig. 3 shows a higher P_2 value is measured for woven ASCs fabricated under longer dissolution times or higher dissolution temperatures. For woven ASCs processed in [C2mim][OAc] at various times and temperatures, a broadly linear increase of the P_2 value was observed.

Fig. 3 indicates that different temperature sets have different rates of dissolution. The equivalence between dissolution time and temperature can be revealed using the TTS principle, by creating a single master curve, which has been widely verified in many polymer systems [32–35]. The implementation of the well-established TTS approach examines the data in natural logarithmic space (ln time), followed by shifting and overlapping the various temperature curves in ln time. A simple multiplicative factor (a_T) could thus relate time and temperature results, as shown in Eqs. (3) and (4).

$$t_R = t_1 a_T \tag{3}$$

$$\ln t_R = \ln t_1 + \ln a_T \tag{4}$$

where T_1 is the temperature of the data set to be shifted, T_R is the chosen reference temperature, t_1 and t_R are the time before and after scaling respectively, and ln a_T is the shift factor in logarithmic space, as schematically illustrated in Fig. 4a. Firstly, a reference temperature was chosen, 50 °C here, as it is in the middle of our temperature range. Secondly, the other temperature sets were shifted along the X axis (ln time) toward this reference set to achieve the best overlap. The amount by which each temperature set was shifted is called the shift factor (ln a_T). Then a polynomial was fitted once a smooth and continuous superimposed data set was formed, the goal here is to vary individual shift factors to maximise the R^2 value between the reference set and each subsequent data set, to provide a best fit where R^2 value is closest to 1. Upon shifting, the final master curve for the variation of the P_2 values for the obtained woven silk composites with ln time shifted to 50 °C is showed in Fig. 4b. Subsequently, P_2 values versus dissolution time is plotted and shown in Fig. 4c. It can be seen that the master curve starts to flatten after 4 h of dissolution at 50 °C.

By plotting the shift factors (ln a_T) versus the inverse absolute temperature, we can evaluate if the rate of the dissolution obeys an Arrhenius-like behaviour, as expressed in Eq. (5) or (6).

$$a_T = A\exp^{-}\frac{E_a}{RT} \tag{5}$$

$$\ln a_T = \ln A - \frac{E_a}{RT} \tag{6}$$

where E_a is the Arrhenius activation energy, R is the gas constant and T is the dissolution temperature. Fig. 4d shows ln a_T vs $1/T$ and clearly indicates a linear relationship. The activation energy of woven silk fabric dissolved in [C2mim][OAc] can therefore be calculated from the gradient of the curve, giving an E_a value of 95 ± 17 kJ/mol.

3.3. Measurement of the volume fraction of the coagulated silk matrix (V_m) in the woven all-silk composites

The solvent [C2mim][OAc] applied to woven silk fabrics can penetrate into silk fibroin and break the intermolecular hydrogen bonds in the crystalline regions, and transform the preferentially aligned crystalline structure into a randomly oriented coagulated fraction, which then forms the matrix of the resulting all silk composite. This was shown from the WAXD azimuthal scans, recall Fig. 3, as the dissolution progressed, the P_2 value was seen to increase from 0.14 to 0.25 which suggests that the content of randomly oriented matrix component was increasing with temperature and time. The partially dissolved woven ASCs are therefore composed of two components, the fibre and the matrix. Extrapolating the master curve of P_2 values (Fig. 4c) backwards to time = 0 gives a value of 0.13, which correlates to the unprocessed woven fabric (P_2 fibre). From the diffraction curve of the coagulated silk film, the P_2 was measured to be 0.25 (P_2 matrix). Next, by assuming a linear mixing rule, as expressed in Eqs. (7) and (8), the coagulated matrix fraction (V_m) of each partially dissolved woven ASC can be quantitatively determined.

$$P_2 = P_2^{fibre}V_{fibre} + P_2^{matrix}V_m \tag{7}$$

Rearranging Eq. (7) to make V_m, the subject leads to

$$V_m = \frac{P_2^{fibre} - P_2^{composite}}{P_2^{fibre} - P_2^{matrix}} \tag{8}$$

Assuming $V_{fibre} + V_m = 1$.

Fig. 5a indicates the coagulated matrix fraction, V_m, for woven ASCs obtained under various dissolution times and temperatures. Longer dissolution times lead to a larger V_m value. As reported above, the woven silk fabric dissolution process exhibits time–temperature equivalence. Similarly, the TTS principle should be applicable for the corresponded

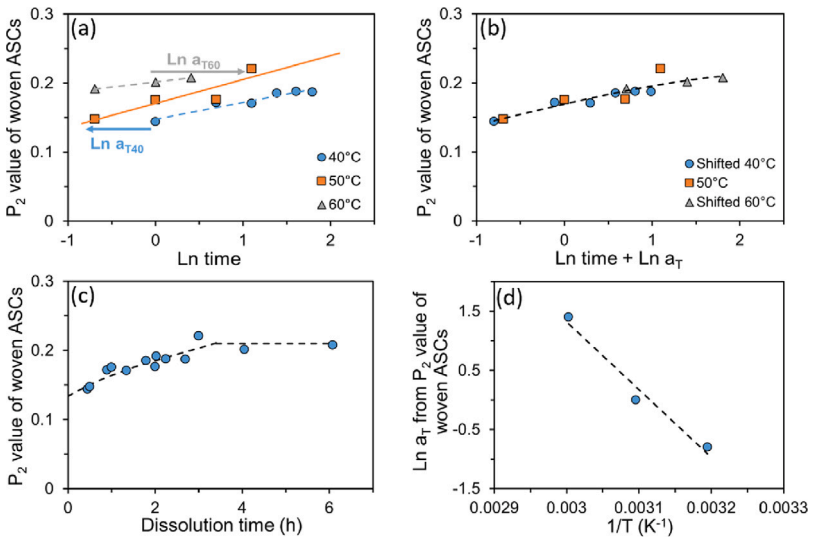

Fig. 4. (a) Shifting P_2 values from different temperature sets in ln space towards the reference temperature set (50 °C), (b) shifted P_2 values generated as a master curve in ln space, (c) its master curve versus dissolution time at 50 °C, (d) shift factors (ln a_T) plotted against inverse temperatures, indicating Arrhenius behaviour; the dashed lines in (a and c) are guide for the eye, and those in (b and d) are second-degree polynomial and linear fitting lines, respectively.

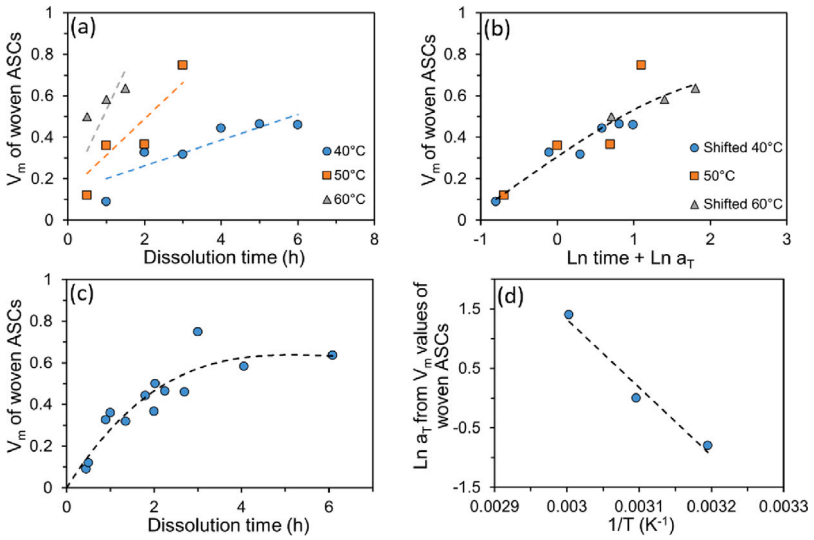

Fig. 5. (a) V_m values at various dissolution times and temperatures, (b) its master curve in ln space, (c) its master curve against dissolution time at 50 °C, (d) its Arrhenius plot; the dashed lines in (a and c) are guide for the eye, and those in (b and d) are second-degree polynomial and linear fitting lines, respectively.

V_m values. Therefore, as showed in Fig. 5b, the demonstrated shifting method is now implemented to generate a master curve of the V_m values for the obtained woven ASCs, again using 50 °C as the reference temperature.

Fig. 5c expresses the master curve of the V_m values from each woven silk composites dissolved in [C2mim][OAc] at various temperatures now plotted with respect to dissolution time, at a reference temperature of 50 °C. It can be observed that up to 50% of woven silk fabrics are dissolved in the first 2 h, and only a further 20% dissolved between 2 to 6 h of dissolution. A significant reduction of dissolution rate can be found. Nevertheless, the dissolution process still obeys TTS principle.

Upon V_m TTS shifting, the obtained shift factors can now be plotted as a function of inverse temperature as before for the P_2 results. In Fig. 5d, a straight line is again found to fit the data points, which indicates the Arrhenius-type behaviour, thus the dissolution of woven silk fabric in [C2mim][OAc] was calculated to have an activation energy of 95 ± 17 kJ/mol. This value is identical to the previous E_a calculated from P_2 TTS analysis, which is to be expected as they are mathematically related to each other.

3.4. Mechanical properties of woven ASCs

Through tensile tests, the mechanical performance of woven ASCs when weft direction is vertical were investigated. The mean values of Young's modulus at a temperature of 40 °C for different dissolution times are shown in Fig.S2. Similar to our previous studies on single silk fibres [29], a 'preformed stage' can also be found during the dissolution of woven silk fabrics. During 0 to 2 h dissolution time [C2mim][OAc] penetrates and flows through the gaps between the multi-filaments, leading to the dissolution of a sufficient amount of silk filaments, that subsequently transforms into matrix on coagulation, to form a close-packed fibre microstructure, which can support an applied stress, through the now bonded filaments and matrix. As a consequence, the maximum Young's modulus of the woven ASC reaches 3.6 GPa. Thereafter, a linear reduction of Young's modulus values can be seen due to fibre cores being dissolved and more matrix created.

The Young's modulus values of woven ASCs obtained from various times and temperatures are shown in Fig. 6a, it is noted that the 'preformed stage' result is removed, since it represents the early stage

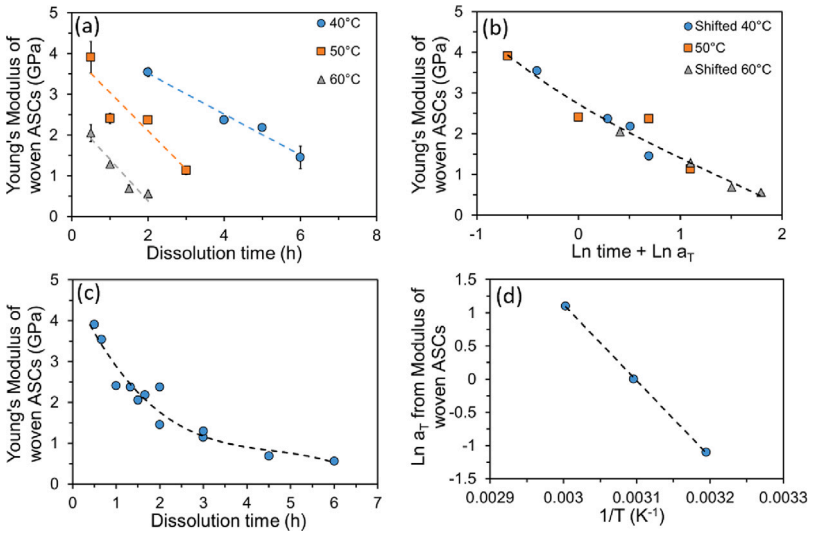

Fig. 6. (a) Young's modulus at various dissolution times and temperatures; (b) its master curve in ln space; (c) its master curve versus dissolution time, at 50 °C, the intercept of this curve gives unprocessed woven silk fabric Young's modulus of 4.7 ± 0.5 GPa; (d) its Arrhenius plot; the dashed lines in (a and c) are guide for the eye, and those in (b and d) are second-degree polynomial and linear fitting lines, respectively.

of dissolution and would have a different activation energy. Fig. 6a demonstrates that the measured woven ASCs Young's modulus continuously decreases, and the rate of decrease becomes more rapid at higher temperatures.

Hence, it is worthwhile to see if the variation of the modulus obeys the TTS principle. After applying the same shifting procedure as introduced above, again using 50 °C as reference temperature, a master curve of Young's modulus values can be seen in Fig. 6b. Modulus values gained from other temperatures were superimposed towards the polynomial curve of the reference temperature set, and constructed a master curve with largest R^2 value. This also suggested that Young's modulus values determined from different temperature sets can be superimposed together through applying certain shift factors ($\ln a_T$). Master curve of Young's modulus values for woven ASCs versus dissolution time at a reference temperature of 50 °C, is shown in Fig. 6c. The measured optimum Young's modulus (4 GPa) is higher than that from all-silk composites fabricated using the two-step method, 3.1 GPa, reported by Yuan et al. [24], and almost comparable to woven silk–epoxy composite (6.5 GPa) reported by Shah et al. [6]. A linear relationship between the shifting factors and inverse temperatures is shown in Fig. 6d, which once again demonstrates Arrhenius-like behaviour. The dissolution activation energy from Fig. 6d was calculated from the gradient of the line, gave a value of 95 ± 2 kJ/mol. This is very close to the previous two values from P_2 and V_m measurements (95 ± 17 kJ/mol).

Tensile strength and elongation at break values of woven ASCs obtained from various times and temperatures were also calculated from their respective stress–strain curves, as shown in Fig. 7a and d. The woven ASC fabricated from 40 °C at 2 h displayed the highest tensile strength (80 ± 7 MPa), which is comparable to the strength value of plain woven silk reinforced with epoxy resin composites (112 ± 2 MPa), as reported in literature [6]. Meanwhile, measured elongation at break (7.9 ± 0.3%) values were greater in comparison to the corresponding literature value (5.2 ± 0.2%). Time–temperature equivalence is again shown in the resulting tensile strength and elongation at break values, both measured parameters exhibited decrease subject to increasing time and temperature. Thus, following the same shifting procedure as described above, different temperature sets were shifted in ln space towards the reference temperature set (50 °C) and generated master curves, given in Fig. 7b and f. Consequently, the changes of tensile strength and elongation at break are displayed versus dissolution time (Fig. 7c and g), these imply that it is possible to design silk fibre reinforced composites with desired mechanical properties through the control of dissolution time and temperature. The shift factors required to construct master curves were again plotted against inverse temperatures and shown in Fig. 7d and h, both having linear dependencies, E_a were subsequently measured at 87 ± 7 kJ/mol and 92 ± 26 kJ/mol from the determined strength and strain values, respectively.

A comparison of the five measured dissolution activation energies results is given in Table.S1. The average value for the dissolution of woven silk composites in [C2mim][OAc] is calculated as 93 ± 2 kJ/mol. It would be of interest to compare the change of V_m over dissolution time for woven and single ASCs processed under the same reference temperature (50 °C was chosen here), result is illustrated in Fig. 8. It is worth to mention, we previously studied the single silk fibre dissolution behaviour in [C2mim][OAc] [29], and it was found that the coagulated matrix fraction (V_m) along single silk fibre can also be quantified by following the orientation (P_2) changes since they are mathematically related to each other through a linear mixing rule. Herein, the master curve of V_m against dissolution time for single ASCs was implemented from our previous work [29], with V_m measured from different temperature sets superimposed to a reference temperature set (50 °C). In Fig. 8, as expected, comparing to single fibre, when impregnating woven fabrics to fabricate ASCs, longer dissolution time needed for woven silk fabrics to achieve the same amount of V_m at the same dissolution temperature.

It is likely that the viscosity of [C2mim][OAc] is increased when impregnating woven fabric compared to single fibre, and the solvent diffusion rate is dramatically decreased in the woven fabric system. In addition, due to the geometry difference, single fibre is expected to expose larger relative contact area to [C2mim][OAc] than the woven fabric which would enable easier access for [C2mim][OAc] to break inter- and intra-hydrogen bonds between silk molecules to conduct the dissolution process, thus results in a much quicker dissolution rate. These might be the possible reasons why lower dissolution rate was observed when dissolving woven silk fabric comparing to single silk fibre. Interestingly, in combination of our previous work on single silk fibres [29], it was found that the dissolution of single silk fibres in [C2mim][OAc] requires more energy (131 ± 8 kJ/mol) than that of woven silk fabrics (93 ± 2 kJ/mol). One of the possible reasons could be the weaving process introduces excessive abrasion which would result in the fabric damage [36], therefore a lower activation energy is observed for the woven silk fabrics.

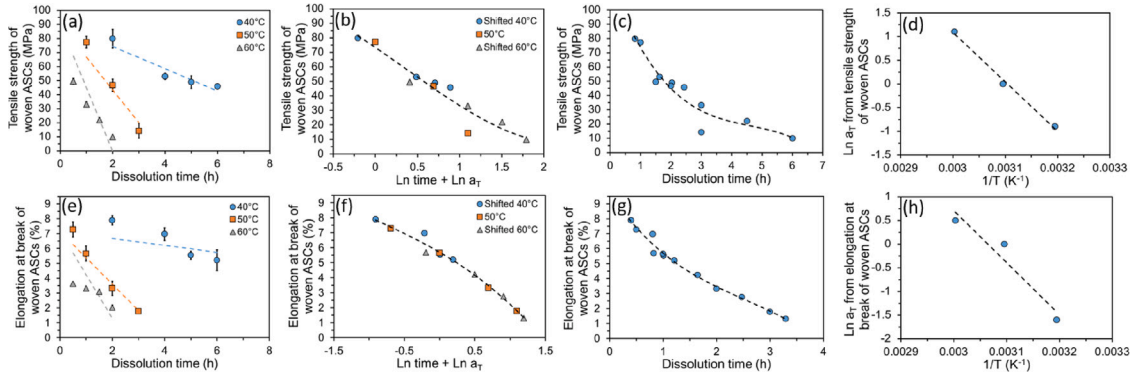

Fig. 7. Breaking strength (a) and elongation at break (e) values at various dissolution times and temperatures, (b)(f) their respective master curves in ln space, (c)(g) their master curves versus dissolution time at 50 °C, (d)(h) their Arrhenius plots; the dashed lines in (a and e) are guide for the eye, and those in (b,c,f,g) are second-degree polynomial, (d and h) are linear fitting lines.

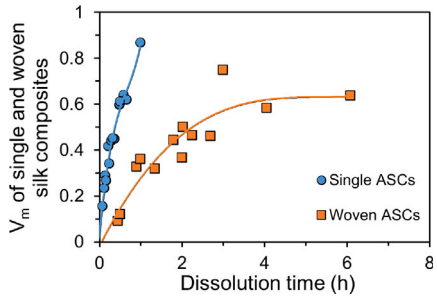

Fig. 8. V_m comparison between woven and single ASCs with respect to dissolution time, at 50 °C; the dashed lines are second-degree polynomial.

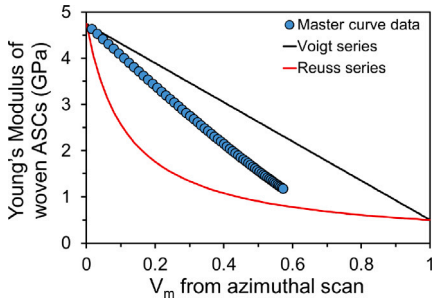

Fig. 9. Young's modulus of woven ASCs plotted against the corresponding V_m, with Voigt and Reuss models to indicate the ROM theory.

3.5. Rule of mixture theory applied on Young's modulus and volume fraction of matrix (V_m)

It would be of interest to see how measured Young's modulus values of each fabricated woven ASC correlate with the V_m, and to assess the applicability of the rule of mixtures (ROM) in our woven composite, as well as evaluate the effect of reinforced fibre volume on the resulting mechanical performance.

Consequently, as showed in Fig. 9, the previously measured master curve of woven ASCs Young's modulus value (Fig. 6c) is plotted against the corresponding V_m master curve values (Fig. 5c). According to the well-established ROM principle, the behaviour of certain properties in a composite material lies within two boundary lines, the Voigt (parallel and upper bound) [37] and Reuss (series and lower bound) [38]. Plotting the two boundary curves requires input of two limiting moduli values, from the ordered unprocessed woven silk fabric and the coagulated SF film (matrix), respectively. The modulus value of unprocessed woven silk fabric is obtained from extrapolating the modulus TTS curve (Fig. 6c), and shows a value of 4.7 ± 0.5 GPa (V_m = 0). While the matrix modulus is acquired from previous three-point bending tests on coagulated SF film, and gave a value of 0.59 ± 0.01 GPa (V_m = 1).

The Voigt series assumes a perfect bonding between fibre and matrix, as well as that both the fibre and matrix are arranged in parallel, so that the strain in each phase will be the same when the stress is loaded axially. Whereas the Reuss series assumes both phases are arranged in series so that the stress in each phase will be equal [39]. It can be noticed that, as expected, all the master curve data points lie between the two boundary lines, and the modulus reduces with the decrease in volume fraction of fibre. Yan et al. [40] reported a similar observation, where they fabricated woven natural fibre/polymer composites using three different fibres including flax, linen and bamboo, comprising the epoxy as matrix, and use Voigt model to predict their theoretical tensile strength and tensile modulus values. They found the tensile modulus values of woven flax/epoxy, woven linen/epoxy and bamboo/epoxy deviated by −12.3%, −15.6% and −8.2%, respectively, from the predicted Voigt model when the fibre volume fraction is ~55%.

4. Summary

In this work, we fabricated single layer woven all silk composite using the partial dissolution method with the ionic liquid 1-ethyl-3-methylimidazolium acetate ([C2mim][OAc]) as the solvent and methanol as the coagulant. The resulting woven ASCs properties were studied using optical microscopy, WAXD azimuthal scans and tensile tests measurements. Here, we reported for the first time using time–temperature superposition principle to quantify the dissolution activation energy of woven silk fabrics with [C2mim][OAc]. Through following the changes in the orientation of crystallites in woven ASCs, and the employment of the second Legendre polynomial function, different P_2 values were obtained from woven ASCs processed at various times and temperatures. In accordance with the TTS principle, the master curve of P_2 obtained from various times and temperatures was constructed. Tracking the amount of matrix generated was achieved by calculating the V_m from the corresponding P_2 values using a linear mixing rule. They were both found to have Arrhenius-type behaviours, and the dissolution rate was increased rapidly at early dissolution hours and slowed down afterwards (Fig. 5c). The dissolution activation energy was calculated to be 95 ± 17 kJ/mol.

The Young's modulus values of each woven ASC were also measured, and the same TTS shifting method was applied. The E_a was calculated from the gradient of the Arrhenius plot, with a value of 95 ± 2 kJ/mol, which is identical to the E_a values acquired from the P_2 dependence. Additionally, measured tensile strength and elongation at break values exhibited time–temperature equivalence and yield another two methods to determine E_a, having values of 87 ± 7 kJ/mol

(strength measurements) and 92 ± 26 kJ/mol (elongation at break measurements). Master curves of Young's modulus (Fig. 6c), tensile strength (Fig. 7c), and elongation at break (Fig. 7g) expressed against dissolution time provide a guidance when designing silk-based composite with desired tensile properties through the control of dissolution time and temperature. Five different methods all point to a very close dissolution activation energy of woven silk fabric in [C2mim][OAc], giving an average value of 93 ± 2 kJ/mol. The measured Young's modulus values of woven ASCs were also correlated with V_m, and found our prepared woven ASCs lie between Voigt and Reuss models. In combination with our previous work on single silk fibres [29], the dissolution rates and activation energies of single silk fibres and woven silk fabrics in [C2mim][OAc] were compared, and it was found that the woven silk fabrics have a much slower dissolution rate with a lower E_a. The relative contact area and the solvent diffusion rate may be the cause of this, since the [C2mim][OAc] is less capable to diffuse into the woven structure. At the same time, the abrasion during the weaving process could cause fabric damage which might lower the E_a. Woven all-silk composites fabricated in this study showed comparably good tensile properties, with the aid of constructed master curves, it is demonstrated that the mechanical properties can be manipulated via changes in dissolution time and temperature. Due to chemical homogeneity and relatively good mechanical properties, woven ASCs may be particularly attractive as composite in engineering and biomedical applications, where biocompatibility and good interfacial bonding are required.

CRediT authorship contribution statement

Xin Zhang: Conceptualization, Methodology, Formal analysis, Investigation, Writing – original draft, Visualization. **Michael E. Ries:** Conceptualization, Writing – review & editing, Supervision, Project administration. **Peter J. Hine:** Conceptualization, Writing – review & editing, Supervision, Project administration.

Declaration of competing interest

The authors declare that they have no known competing financial interests or personal relationships that could have appeared to influence the work reported in this paper.

Data availability

Data will be made available on request.

Acknowledgements

The authors would like to acknowledge the support from Dr. Daniel L. Baker, for experiment training and valuable discussions. Dr. James E. Hawkins, Dr. Yunhao Liang and Maer Hael are gratefully acknowledged for their help and discussions. The data associated with this paper are openly available from the University of Leeds Data Repository. https://doi.org/10.5518/1191

Funding

This research did not receive any specific grant from funding agencies in the public, commercial, or not-for-profit sectors.

Appendix A. Supplementary data

Supplementary material related to this article can be found online at https://doi.org/10.1016/j.compscitech.2023.110046.

References

[1] Y.G. Thyavihalli Girijappa, S. Mavinkere Rangappa, J. Parameswaranpillai, S. Siengchin, Natural fibers as sustainable and renewable resource for development of eco-friendly composites: A comprehensive review, Front. Mater. 6 (2019) 226.
[2] P. Peças, H. Carvalho, H. Salman, M. Leite, Natural fibre composites and their applications: A review, J. Compos. Sci. 2 (4) (2018) http://dx.doi.org/10.3390/jcs2040066.
[3] K. Pickering, M.A. Efendy, T. Le, A review of recent developments in natural fibre composites and their mechanical performance, Composites A 83 (2016) 98–112, http://dx.doi.org/10.1016/j.compositesa.2015.08.038, Special Issue on Biocomposites.
[4] A. Ude, R. Eshkoor, R. Zulkifili, A.K. Ariffin, D. Abd Wahab, C. Azhari, Bombyx mori silk fibre and its composite: A review of contemporary developments, Mater. Des. 57 (2014) 298–305, http://dx.doi.org/10.1016/j.matdes.2013.12.052.
[5] D. Shah, Developing plant fibre composites for structural applications by optimising composite parameters: A critical review, J. Mater. Sci. 48 (2013) 6083–6107, http://dx.doi.org/10.1007/s10853-013-7458-7.
[6] D.U. Shah, D. Porter, F. Vollrath, Can silk become an effective reinforcing fibre? A property comparison with flax and glass reinforced composites, Compos. Sci. Technol. 101 (2014) 173–183.
[7] J. Melke, S. Midha, S. Ghosh, K. Ito, S. Hofmann, Silk fibroin as biomaterial for bone tissue engineering, Acta Biomater. 31 (2016) 1–16, http://dx.doi.org/10.1016/j.actbio.2015.09.005.
[8] H.-Y. Wang, Z.-G. Wei, Y.-Q. Zhang, Dissolution and regeneration of silk from silkworm bombyx mori in ionic liquids and its application to medical biomaterials, Int. J. Biol. Macromol. 143 (2020) 594–601, http://dx.doi.org/10.1016/j.ijbiomac.2019.12.066.
[9] S. Inoue, K. Tanaka, F. Arisaka, S. Kimura, K. Ohtomo, S. Mizuno, Silk fibroin of Bombyx mori is secreted, assembling a high molecular mass elementary unit consisting of H-chain, L-chain, and P25, with a 6:6:1 molar ratio, J. Biol. Chem. 275 (51) (2000) 40517–40528, http://dx.doi.org/10.1074/jbc.M006897200.
[10] E. Sashina, A. Bochek, N. Novoselov, D. Kirichenko, Structure and solubility of natural silk fibroin, Russ. J. Appl. Chem. 79 (2006) 869–876, http://dx.doi.org/10.1134/S1070427206060012.
[11] J. Dupont, From molten salts to ionic liquids: A "Nano" journey, Acc. Chem. Res. 44 (11) (2011) 1223–1231, http://dx.doi.org/10.1021/ar2000937.
[12] D. Fort, R. Remsing, R. Swatloski, P. Moyna, G. Moyna, R. Rogers, Can ionic liquids dissolve wood? Processing and analysis of lignocellulosic materials with 1-n-butyl-3-methylimidazolium chloride, Green Chem. 9 (1) (2007) 63–69, http://dx.doi.org/10.1039/b607614a.
[13] J. Hou, Z. Zhang, L. Madsen, Cation/anion associations in ionic liquids modulated by hydration and ionic medium, J. Phys. Chem. B 115 (16) (2011) 4576–4582, http://dx.doi.org/10.1021/jp1110899.
[14] R.P. Swatloski, S.K. Spear, J.D. Holbrey, R.D. Rogers, Dissolution of cellose with ionic liquids, J. Am. Chem. Soc. 124 (18) (2002) 4974–4975, http://dx.doi.org/10.1021/ja025790m, PMID: 11982358.
[15] Y. Qin, X. Lu, N. Sun, R.D. Rogers, Dissolution or extraction of crustacean shells using ionic liquids to obtain high molecular weight purified chitin and direct production of chitin films and fibers, Green Chem. 12 (2010) 968–971, http://dx.doi.org/10.1039/C003583A.
[16] S. Zheng, Y. Nie, S. Zhang, X. Zhang, L. Wang, Highly efficient dissolution of wool keratin by dimethylphosphate ionic liquids, ACS Sustain. Chem. Eng. 3 (11) (2015) 2925–2932, http://dx.doi.org/10.1021/acssuschemeng.5b00895.
[17] D. Phillips, L. Drummy, D. Conrady, D. Fox, R. Naik, M. Stone, P. Trulove, H. De Long, R. Mantz, Dissolution and regeneration of bombyx mori silk fibroin using ionic liquids, J. Am. Chem. Soc. 126 (44) (2004) 14350–14351, http://dx.doi.org/10.1021/ja046079f.
[18] J.G. Hardy, L.M. Römer, T.R. Scheibel, Polymeric materials based on silk proteins, Polymer 49 (20) (2008) 4309–4327, http://dx.doi.org/10.1016/J.POLYMER.2008.08.006.
[19] D.U. Shah, D. Porter, F. Vollrath, Opportunities for silk textiles in reinforced biocomposites: Studying through-thickness compaction behaviour, Composites A 62 (2014) 1–10, http://dx.doi.org/10.1016/J.COMPOSITESA.2014.03.008.
[20] Q.T. Shubhra, M. Saha, A. Alam, M. Beg, M.A. Khan, Effect of matrix modification by natural rubber on the performance of silk-reinforced polypropylene composites, J. Reinf. Plast. Compos. 29 (22) (2010) 3338–3344, http://dx.doi.org/10.1177/0731684410375640.
[21] A.W. Van Vuure, J. Vanderbeke, Y. Mosleh, I. Verpoest, N. El-Asmar, Ductile woven silk fibre thermoplastic composites with quasi-isotropic strength, Composites A 147 (2021) 106442, http://dx.doi.org/10.1016/j.compositesa.2021.106442.
[22] Y. Xie, C.A. Hill, Z. Xiao, H. Militz, C. Mai, Silane coupling agents used for natural fiber/polymer composites: A review, Composites A 41 (7) (2010) 806–819.
[23] X. Zhao, K. Copenhaver, L. Wang, M. Korey, D.J. Gardner, K. Li, M.E. Lamm, V. Kishore, S. Bhagia, M. Tajvidi, et al., Recycling of natural fiber composites: Challenges and opportunities, Resour. Conserv. Recy. 177 (2022) 105962.
[24] Q. Yuan, J. Yao, X. Chen, L. Huang, Z. Shao, The preparation of high performance silk fiber/fibroin composite, Polymer 51 (21) (2010) 4843–4849, http://dx.doi.org/10.1016/j.polymer.2010.08.042.

[25] P. Laity, C. Holland, Thermo-rheological behaviour of native silk feedstocks, Eur. Polym. J. 87 (2017) 519–534, http://dx.doi.org/10.1016/j.eurpolymj.2016.10.054.

[26] Y. Liu, L. Yang, C. Ma, Thermal analysis and kinetic study of native silks, J. Therm. Anal. Calorim. 139 (1) (2020) 589–595, http://dx.doi.org/10.1007/s10973-019-08420-4.

[27] Q. Liu, F. Wang, Y. Li, H. Yu, Q. Ma, Z. Gu, Comparative studies of structure, thermal decomposition mechanism and thermodynamic parameters of two kinds of silk fibroin films, Sci. Sin. Chim. 49 (7) (2019) 1014–1029, http://dx.doi.org/10.1360/N032018-00265.

[28] I.C. Um, H.Y. Kweon, K.G. Lee, D.W. Ihm, J.H. Lee, Y.H. Park, Wet spinning of silk polymer: I. Effect of coagulation conditions on the morphological feature of filament, Int. J. Biol. Macromol. (ISSN: 01418130) 34 (1–2) (2004) http://dx.doi.org/10.1016/j.ijbiomac.2004.03.007.

[29] X. Zhang, M.E. Ries, P.J. Hine, Time–temperature superposition of the dissolution of silk fibers in the ionic liquid 1-ethyl-3-methylimidazolium acetate, Biomacromolecules 22 (3) (2021) 1091–1101, http://dx.doi.org/10.1021/acs.biomac.0c01467, PMID: 33560832.

[30] J. Warwicker, The crystal structure of silk fibroin, Acta Crystallogr. 7 (8–9) (1954) 565–573.

[31] J. Hermans, P. Hermans, D. Vermaas, A. Weidinger, Quantitative evaluation of orientation in cellulose fibres from the X-ray fibre diagram, Recl. Trav. Chim. Pays-Bas 65 (6) (1946) 427–447, http://dx.doi.org/10.1002/recl.19460650605.

[32] J. Ferry, Viscoelastic properties of polymers, 1980.

[33] A. Amiri, C. Ulven, S. Huo, Effect of chemical treatment of flax fiber and resin manipulation on service life of their composites using time-temperature superposition, Polymers 7 (10) (2015) 1965–1978, http://dx.doi.org/10.3390/polym7101493.

[34] J. Hawkins, Y. Liang, M. Ries, P. Hine, Time temperature superposition of the dissolution of cellulose fibres by the ionic liquid 1-ethyl-3-methylimidazolium acetate with cosolvent dimethyl sulfoxide, Carbohydr. Polym. Technol. Appl. 2 (2021) http://dx.doi.org/10.1016/j.carpta.2020.100021.

[35] Y. Liang, J. Hawkins, M. Ries, P. Hine, Dissolution of cotton by 1-ethyl-3-methylimidazolium acetate studied with time–temperature superposition for three different fibre arrangements, Cellulose 28 (2) (2021) 715–727, http://dx.doi.org/10.1007/s10570-020-03576-x.

[36] Y.E. Elmogahzy, Finished fibrous assemblies, Eng. Text. (2020) 275–298, http://dx.doi.org/10.1016/B978-0-08-102488-1.00011-3.

[37] W. Voigt, Ueber die Beziehung zwischen den beiden Elasticitätsconstanten isotroper Körper, Ann. Phys. 274 (12) (1889) 573–587, http://dx.doi.org/10.1002/andp.18892741206.

[38] A. Reuss, Berechnung der Fließgrenze von Mischkristallen auf Grund der Plastizitätsbedingung für Einkristalle, ZAMM - J. Appl. Math. Mech. / Z. Angew. Math. Mech. 9 (1) (1929) 49–58, http://dx.doi.org/10.1002/zamm.19290090104.

[39] D. Hull, T.W. Clyne, Elastic deformation of long-fibre composites, in: An Introduction To Composite Materials, second ed., in: Cambridge Solid State Science Series, Cambridge University Press, 1996, pp. 60–77, http://dx.doi.org/10.1017/CBO9781139170130.006.

[40] L. Yan, N. Chouw, X. Yuan, Improving the mechanical properties of natural fibre fabric reinforced epoxy composites by alkali treatment, J. Reinf. Plast. Compos. 31 (6) (2012) 425–437, http://dx.doi.org/10.1177/0731684412439494.